DIRT/3D: 3D phenotyping for maize (*Zea mays*) root architecture in the field

Suxing Liu[1,2,3], Carlos Sherard Barrow[4], Meredith Hanlon[5], Jonathan P. Lynch[5], Alexander Bucksch*[1,2,3]

[1] Department of Plant Biology, University of Georgia, Athens, GA, United States

[2] Warnell School of Forestry and Natural Resources, University of Georgia, Athens, GA, United States

[3] Institute of Bioinformatics, University of Georgia, Athens, GA, United States

[4] Instrumentation Shop, University of Georgia, Athens, GA, United States

[5] Department of Plant Science, Penn State University, State College, PA, United States

*corresponding author

Abstract

The development of crops with deeper roots holds substantial promise to mitigate the consequences of climate change. Deeper roots are an essential factor to improve water uptake as a way to enhance crop resilience to drought, to increase nitrogen capture to reduce fertilizer inputs and to increase carbon sequestration from the atmosphere to improve soil organic fertility. A major obstacle to achieving these improvements is the bottleneck in the high-throughput phenotyping of field-grown roots. We address this bottleneck with DIRT/3D, a newly developed image-based 3D root phenotyping platform, which measures 16 architecture traits in mature maize root systems. DIRT/3D computed reliably all 16 traits on a test panel of 12 contrasting maize genotypes. The analysis of the maize panel validated traits such as distance between whorls, and the number, angle, and diameters of crown and brace roots. Overall, we observed a coefficient of determination of r^2>0.84 and a high broad-sense heritability of H^2_{mean}> 0.7 for all traits. Means of the 16 traits and a newly developed descriptor to characterize a complete root architecture distinguished all genotypes. DIRT/3D is a step towards automated quantification of highly occluded maize root systems in the field and will support breeders and root biologists to improved carbon sequestration and food security in the face of the adverse effects of climate change.

Introduction

Evaluating the information encoded in the shape of a plant as a response to environments is essential to understand the function of plant organs (Bucksch 2011). In particular, roots exhibit shape diversity that is measurable as variation in rooting angles, numbers of roots per type, length, or diameter of roots within a root system (Lynch and Brown 2012). An understanding of variation in root systems facilitates breeding for favorable root characteristics to improve yield in suboptimal conditions, including those resulting from climate change (Lynch 2013). Improving root phenotypes through crop breeding and management holds promise for improved food security in developing nations, where drought, low soil fertility and biotic constraints to root function are primary causes of low yields, and also for reducing the environmental impacts of intensive agriculture by reducing the need for intensive fertilization and irrigation (Lynch 2019). Root traits also offer opportunities to improve C sequestration (Paustian, Lehmann et al. 2016). These challenges demand efforts across a range of disciplines, from mathematics over computer science to plant biology and applied fields like plant breeding and agronomy (Bucksch, Atta-Boateng et al. 2017, Bucksch, Das et al. 2017).

A major interdisciplinary challenge in root biology is the development of deeper rooting crop varieties. Deeper roots promise a three-fold impact: they improve drought resilience, lower fertilizer input, and decrease atmospheric carbon. Deeper roots improve drought resilience to stronger and more frequently occurring droughts (Ault 2020) by tapping into water in deep soil domains (Lynch and Wojciechowski 2015). Nitrogen capture increases when roots grow deeper because nitrogen diffuses into and accumulates in deeper soil layers (Lynch 2019). Deeper rooting crops increase carbon sequestration (Smith, Martino et al. 2007) mostly by depositing more organic residues in soils, thereby replenishing carbon after harvest (Paustian, Agren et al. 1997). An important tool in breeding deeper roots is the large-scale automated evaluation of root traits in the highly occluded root system architecture (Topp, Bray et al. 2016). Maize (*Zea mays*) in particular, with over 700 Mt of maize production world-wide (Ranum, Peña-Rosas et al. 2014), is a prime target for improving rooting depth. However, measuring important root traits for deeper rooting in maize is hampered by the availability of advanced root phenotyping methods on the field-scale (Kuijken, van Eeuwijk et al. 2015). Therefore, the research community has pushed for the development of a root phenotyping system that operates under field conditions (Paez-Garcia, Motes et al. 2015).

The field vs. lab complement

The majority of existing phenotyping methods to evaluate root architecture non-destructively emerged from laboratory settings. These methods range from fully automatic (Galkovskyi, Mileyko et al. 2012) to manually assisted (Lobet, Pagès et al. 2011) and consider a variety of growth systems like gel cylinders (Iyer-Pascuzzi, Symonova et al. 2010), rhizotrons (Nagel, Putz et al. 2012, Rellán-Álvarez, Lobet et al. 2015), mesocosms (Nagel, Putz et al. 2012) and germination paper (Falk, Jubery et al. 2020). Root phenotyping under lab conditions necessitates the use of constrained growth containers (Poorter, Bühler et al. 2012, Bourgault, James et al. 2017), artificial growth media (Oliva and Dunand 2007), and environments that potentially alter root system architecture (de Dorlodot, Bertin et al. 2005, Draye, Thaon et al. 2018). Therefore, it is essential to translate phenotyping experiments from the lab into repeatable field experiments (Zhu, Ingram et al. 2011, Bucksch, Burridge et al. 2014, Poorter, Fiorani et al. 2016).

In contrast, root phenotyping in the field is currently either invasive or destructive. Invasive procedures record small sections of the root with minirhizotron cameras placed in the soil (Gray, Strellner et al. 2013, Yu, Zare et al. 2019). Still, these procedures are incapable of recording the full root system. Therefore, investigating root system architecture relies heavily on the destructive excavation of the root crown. Shovelomics is the standard field-ready protocol to excavate root systems in the field (Trachsel, Kaeppler et al. 2011). It was initially developed for maize and undergoes a constant refinement by the root research community (Zheng, Hey et al. 2020). Other crops, including common bean (*Phaseolus vulgaris*) and cowpea (*Vigna unguiculata*) (Burridge, Jochua et al. 2016), wheat (*T. aestivum*) (Slack, York et al. 2018, York, Slack et al. 2018), rapeseed (*Brassica napus*) (Arifuzzaman, Oladzadabbasabadi et al. 2019) and cassava (*Manihot esculenta*) (Kengkanna, Jakaew et al. 2019) have specialized

shovelomics protocols in place. However, the manual excavation of the crown root system, followed by visual scoring and manual trait measurement, is difficult and subjective to the researcher.

Digital imaging of root traits in 2D

In response, software to measure root traits in simple digital images became available. Approaches to record root traits in the field use different methods in terms of software platforms and imaging setups. The largest software platform is DIRT (Das, Schneider et al. 2015), which provides online image processing for over 650 users following an easy to reproduce imaging protocol. For imaging, DIRT needs a tripod, a consumer camera, and a black background with a white circle. Just recently, DIRT enabled projects associated with root architecture and micronutrient content (Busener, Kengkanna et al. 2020), discovered unknown gene functions (Bray and Topp 2018) and translated traits from the lab to the field (Salungyu, Kengkanna et al. 2020). More sophisticated and expensive imaging setups use specialized tents (Colombi, Kirchgessner et al. 2015) and carefully designed imaging boxes (Grift, Novais et al. 2011, Seethepalli, Guo et al. 2019), along with computationally cheap traits, for use on personal computers. The user can, therefore, choose a system that suits the project needs. Systems generally vary in the number of instruments, tools, and samples transported between the lab and field site, as well as the cost of the imaging setup and hardware requirements. However, all these systems share a single obstacle: Resolving the highly occluded branches of a dense 3D root system. The occlusion challenge arises when the 2D image projection of the 3D branching structure 'hides' information of branching locations. Hence, the branching information is unrecoverable and lost.

Digital imaging of root traits in 3D

3D approaches are capable of resolving even highly occluded branching structures (Bucksch 2014). Gel systems were among the first methods to measure fully resolved 3D root systems of younger roots (Clark, MacCurdy et al. 2011, Topp, Iyer-Pascuzzi et al. 2013) and to capture some of their growth dynamics (Symonova, Topp et al. 2015). The bottleneck of imaging and measuring older root systems in constrained growth containers filled with soil, however, remained. Therefore, X-Ray computed tomography (CT) became a widely used tool to phenotype roots in pots filled with soil and soil-like substrates (Pfeifer, Kirchgessner et al. 2015). These lab developments revealed for example new characteristics in maize root development (Jiang, Floro et al. 2019). The X-ray CT approach is, in its applications, comparable to magnetic resonance imaging (MRI) (Metzner, Eggert et al. 2015). MRI also provides a 3D model of the root (van Dusschoten, Metzner et al. 2016) and can be used for time-lapse imaging of growth processes (Jahnke, Menzel et al. 2009). The benefits of both X-Ray CT and MRI are substantial and subject to scientific discussion (Fischer, Lasser et al. 2016). However, both technologies do not meet the needs for large-scale field studies: Firstly, both technologies restrict plant growth to the size of a given growth container. The restriction to smaller sizes is proportional to higher achievable resolution. Therefore, it is common to observe an immature "pot phenotype" instead of a relevant phenotype grown in field soils (Poorter, Bühler et al. 2012, Bourgault, James et al. 2017). Secondly, both methods are relatively slow and typically take 30 minutes or more to collect root imaging data. Extremes of several days are reported for X-Ray CT systems to achieve the resolution of root hairs (Keyes, Daly et al. 2013, Sozzani, Busch et al. 2014). An additional constraint is the cost of constructing, operating, and staffing such facilities, few of which are devoted to root studies.

In response to these phenotyping limitations, we developed DIRT/3D as an automatic 3D root phenotyping system for excavated root systems grown in agricultural fields. Our approach consists of a newly developed 3D root scanner and root analysis software. The 3D root scanner captures image data of one excavated maize root in about 5 minutes. Our software uses the image data to produce a colored 3D point cloud model and to compute 16 root traits. The computed traits measure individual roots and also characterize the complete root system. Individual root traits include number, angle, and diameters of crown and brace roots. Traits like eccentricity or the distance between brace and crown root whorls characterize the root system. We also introduce a new 3D whole root descriptor that encodes the arrangement of roots within the root system.

Results

DIRT/3D enables automatic measurement of 3D root traits for field-grown maize

We developed DIRT/3D (Digital Imaging of Root Traits in 3D) system to phenotype excavated root crowns of maize (Figure 1). The system includes a 3D root scanner and a suite of parameter-free software that reconstructs field-grown maize roots as a 3D point cloud model. The software also contains algorithms to compute 16 root traits.

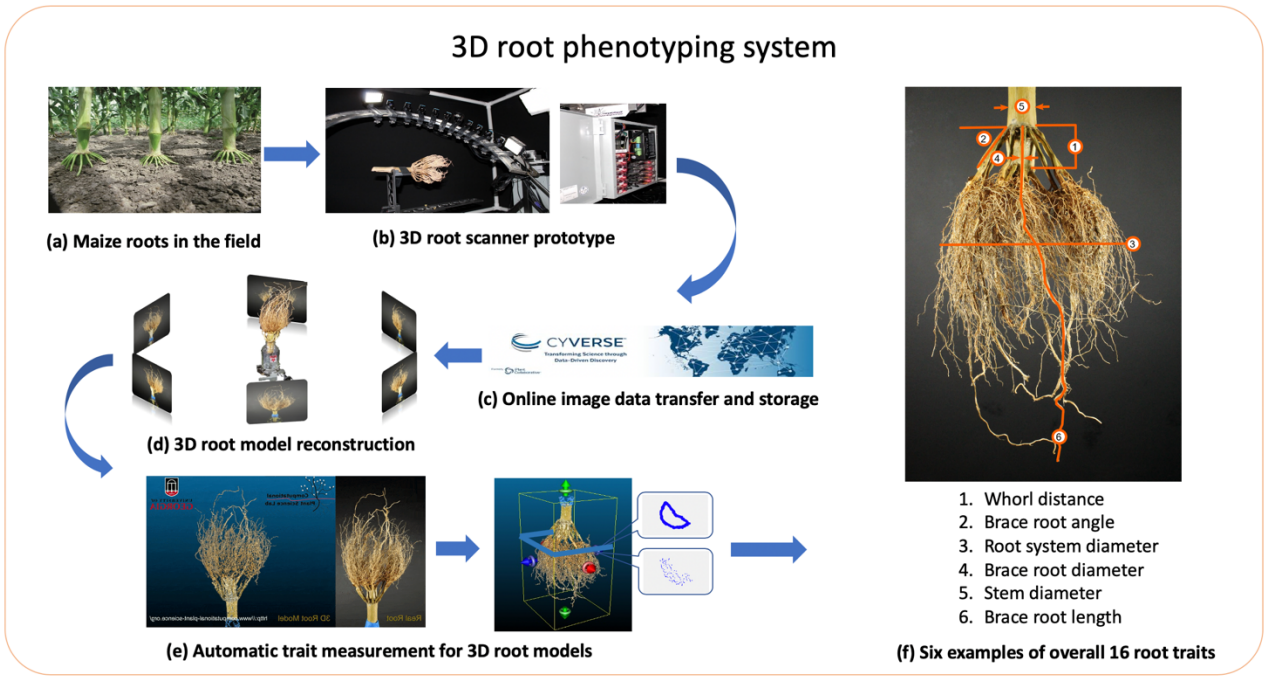

Figure 1: Schematic overview of our DIRT/3D system. The 3D root scanner (b) fits roots grown in the field (a) and excavated with the Shovelomics protocol (Trachsel, Kaeppler et al. 2011). The scanner, with ten synchronized industrial cameras mounted on a curved frame, acquires about 2000 images of the root. The images are transferred to and stored in the Cyverse Data Store (Merchant, Lyons et al. 2016) (c). The 3D reconstruction is computed with DIRT/3D's structure-from-motion software (d) and yields the resulting 3D root model (e). Overall, the analysis software calculates 16 root traits from the 3D point cloud of the root system. The image in (f) shows examples for the trait classes angle, diameter, and length. All developed software methods are open source and executable as a Singularity container (Kurtzer, Sochat et al. 2017) on high-performance-computing systems.

The 3D root scanner (Figure 2) utilizes ten industrial cameras mounted on a rotating curved frame (Figure 2a) to capture images from all sides of the maize root (Supplementary Material 1). Scanning of one maize root completes in five minutes. After obtaining the image data, we reconstruct a 3D point cloud of the root system (Figure 3A). By analyzing thin level sets of the 3D point cloud, DIRT/3D revealed traits behind multiple layers of occlusions (Detailed pipeline in Supplementary Material 2). For example, DIRT/3D measures the distance between the brace and crown root whorl and the number of brace and crown roots. DIRT/3D also tracks every individual root within the root system, starting from the stem down to the emerging lateral in the excavated root crown. Each individually tracked root enables the measurement of numbers, angles, and diameters at the individual root level (Figure 1f).

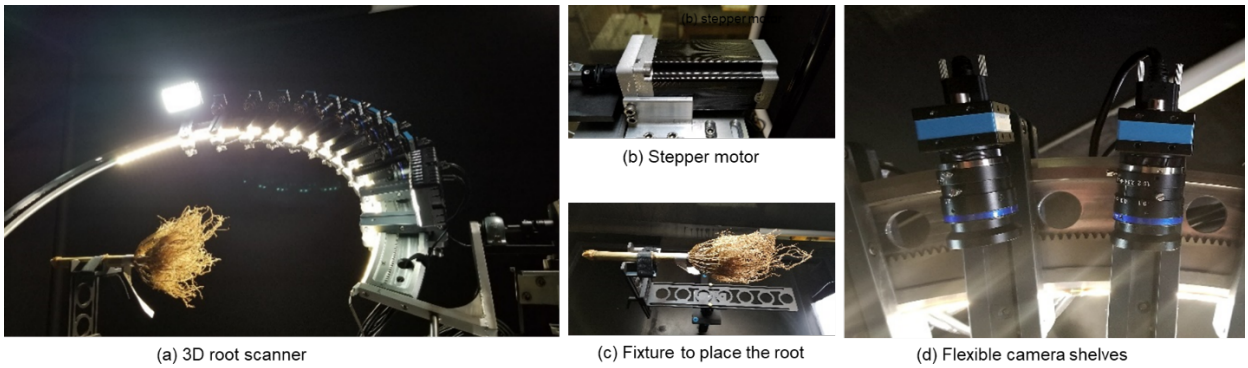

Figure 2: 3D root scanner prototype. (a) 3D root scanner captures images of an excavated maize root grown under field conditions. (b) The stepper motor rotates the curved metal frame with the mounted cameras around the root. (c) The fixture keeps the root in place during scanning. (d) The adjustable camera shelves allow for the free positioning of each camera. The CAD drawings of the 3D root scanner are available in Supplemental Material 3.

We used a panel of 12 maize genotypes with 5-10 replicates per genotype to validate the DIRT/3D pipeline. For our validation trial, the 3D root scanner captured images at pan intervals of 1 degree and tilt intervals of 10 degrees. Figure 3B shows a visual comparison of the captured root architectural variation between the genotypes.

A Detailed views of 3D root model

Figure 3: The automatic DIRT/3D pipeline generates a detailed 3D point cloud, root models. A. The 3D reconstruction of the maize root architecture using 2000 images (including side view from the bottom, side view from the top, front view, bottom view, and top view). The resolution of each image is 3872 pixels × 2764 pixels. The resulting point cloud contains 439.918 points (Supplementary Material 4). B. Comparison between excavated maize root systems and their 3D models: Examples of excavated maize root crowns and their 3D models from a test panel of 12 genotypes. We captured 2D images of the original root sample for each genotype. We built corresponding 3D root models (ply point cloud format) from 2D image data using our automatic parameter-free algorithms. Visual comparison of the 2D views of real roots and their respective 3D root models shows that root architecture, along with the color, is reconstructed (Supplementary Material 5). All 3D models used in the paper are available as .ply file in Supplementary Material 18.

Level set scanning enables extraction of traits from 3D root models

We developed a new method to perform a top-down level set scan of the 3D root model to compute 3D root traits. For a vertically aligned model, we slice the 3D root model from top to bottom at consecutive depth levels (Figure 4). The imaging volume of the scanner is constant, and therefore the number of slices per root is variable. Two benefits result from the fixed scanning volume. First, the transformation to mm is constant, and second, the optimal slice thickness can be determined experimentally for all roots. Therefore, all parameters are constants in the algorithm. Here, a level set image is the vertical 2D projection of each slice onto a plane (Cochard, Delzon et al. 2015, Dinas, Nikaki et al. 2015, Hyun, Bae et al. 2016) representing the sequential distribution of roots into deeper soil levels (Figure 4 (b)-(e)).

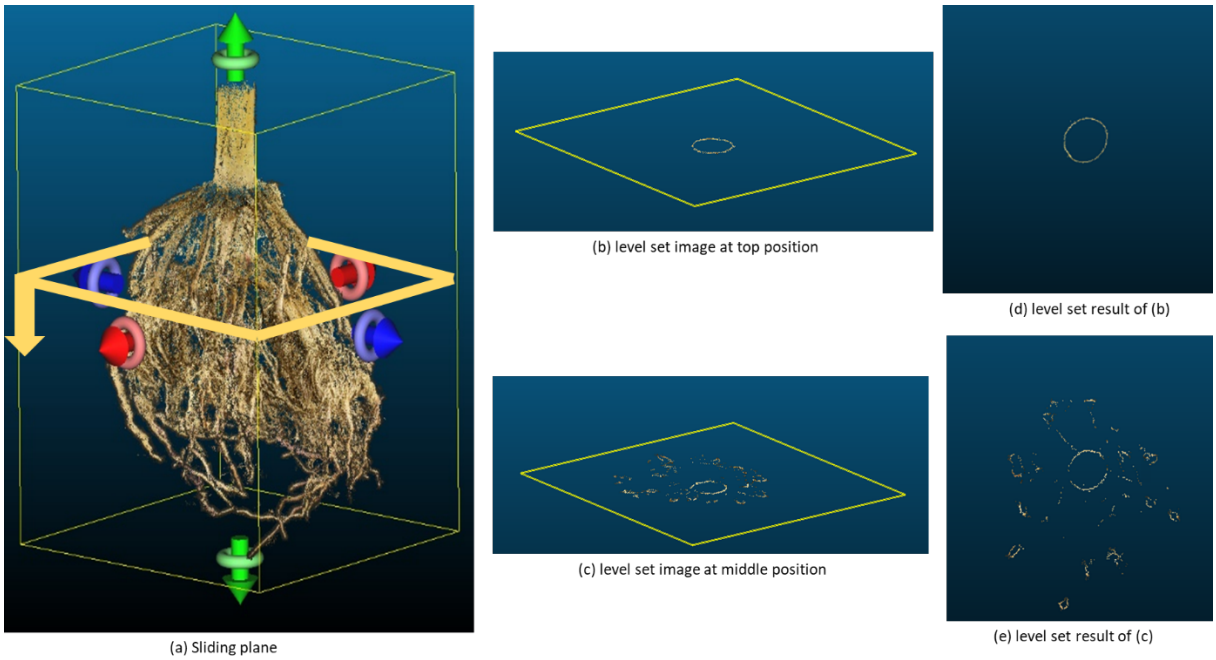

Figure 4: The level set image sequence for the estimation of root traits. (a) A sliding plane scans the 3D root model from top to bottom to acquire a level set image sequence. The information content per level set image varies with depth and generally encodes the points at a pre-defined distance to the sliding plane. For example, at the top (b and d), only information about the stem appears in the level set image. At a middle position (c and e), individual roots are visible as additional circles.

Ideally, each root is a closed circle in the level set plane. However, roots are under-sampled or affected by noise such that the contours of some roots are disconnected. A video sequence of all level set images would result in a flickering effect. Therefore, we use a phase-based frame interpolation technique (Meyer, Wang et al. 2015) to smooth the level set image sequence. This method estimates transition frames between the level set images, which is equal to an up-sampling process of the 3D point cloud (Waki 2016). Insufficient sampled locations of the root models are interpolated, which results in a smooth connection of formerly disconnected contours on level set images (Zhao, He et al. 2018). A comparison of the original and smoothened sequence of level set images shows the increased density of the 3D root model (Supplementary Material 6).

The active contour snake model identifies individual roots per level set image

The image sequence of the smoothened level sets is the key to compute the location and size parameters of individual roots. Applying the active contour snake model (Kass, Witkin et al. 1988) to each level set image results in a curve that circumscribes each individual root in the level set image (Mugerwa, Rey et al. 2019). Each curve contracts and moves towards the closed boundaries of an individual root by minimizing a partial differential

equation, where image boundaries represent a low energy state for the active contour. The partial differential equations formulize a trade-off between an internal and external energy term. The internal energy describes the continuity and smoothness of the contour to controls for curve deformations, and an external energy that describes how well the contour fits the individual root (Zhao, He et al. 2018).

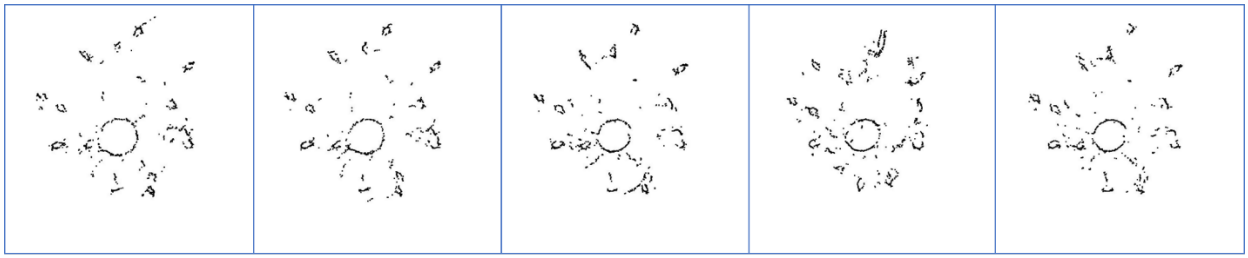

(a) Five sample images from smoothed level set image sequence

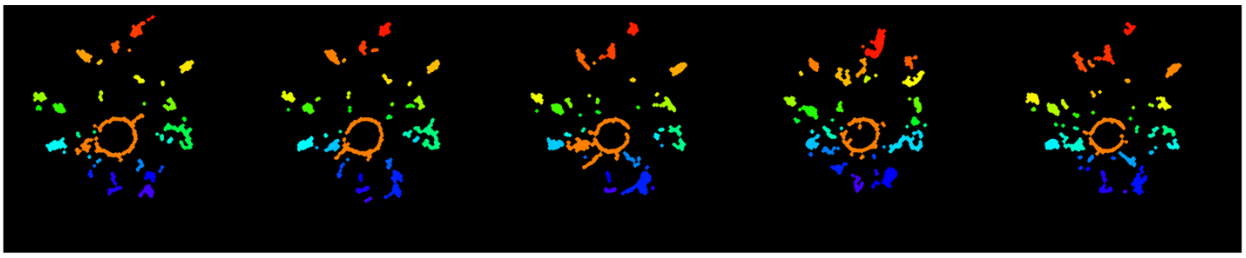

(b) Active snake results of (a)

Figure 5: Active contour snake method identifies individual roots by analyzing connected components. (a) shows five sample images from the smoothened level set images. (b) shows the corresponding results from the active contour snake method. Each extracted individual root is color-coded with connected component labeling. The active contour snake model detects individual roots in each level set image. A video showing the active contour snake evolving process is available in Supplementary Material 7.

Our algorithm initializes a circle around each individual root in each level set as an initial input to the minimization of the active contour snake (Supplementary Material 8). During the iterative minimization of the energy function, we use a periodic boundary condition to enforce a closed curve. The resulting closed boundary curves represent first estimates of individual roots and used as input to compute a binary mask for each level set image sequence using Otsu's binarization method (Moghaddam and Cheriet 2012). We adopt the connected components labeling method to distinguish and label each closed-boundary object, representing individual roots (Playne and Hawick 2018). The result of connected components labeling is a multiple segmentation of individual roots represented by colored components (Figure 5).

However, due to the complexity of the maize root system, roots intertangle or adhere to each other. In an image of the level set sequence, the entanglement will be visible as one connected component instead of two distinct components. We use the watershed segmentation to segment the overlapping root (Supplementary Material 9). The idea behind the watershed algorithm is to interpret grey values in the image as a local topography or elevation. The algorithm uses pre-computed local minima to flood basins around them. The algorithm terminates the flooding of a basin when the watershed lines of two basins meet. The Euclidean Distance Transform (EDT) of the image allows for direct detection of the local minima (Fabbri, Costa et al. 2008). In that way, watersheds assign each pixel to a unique component and allows the distinction entangled roots per level set image (Roshanian, Yazdani et al. 2016).

A combination of Kalman filters and the Hungarian algorithm tracks individual roots

We developed an individual root tracking method by adopting a combination of Kalman filters and the Hungarian algorithm (Sahbani and Adiprawita 2016). The algorithm detects individual roots for consecutive level set images. Once individual roots are detected, the Hungarian algorithm matches the corresponding individual roots across the level set images. To improve the speed of the Hungarian algorithm, we use a Kalman filter to predict matching

individual roots in consecutive level set images (Figure 6). Behind the scenes, the tracking algorithm builds a mathematical model of expected depth development of the root. In doing so, the algorithm uses the current position, relative speed, and acceleration of individual roots to predict their location in the following level set image.

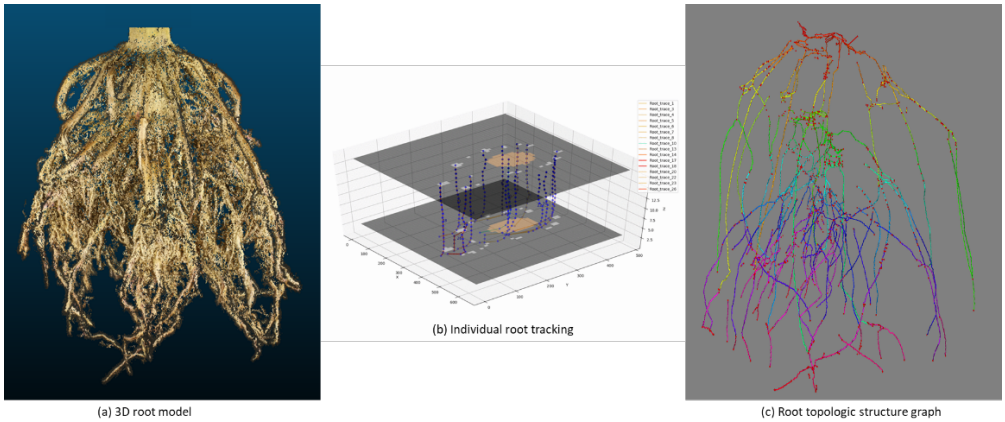

Figure 6: A combination of Kalman filters and the Hungarian algorithm tracks individual roots in the root system. (a) 3D model of a field-grown maize root generated by the DIRT/3D reconstruction. (b) Visualization of the tracking process of individual roots from level set images. Two level set images are visualized with 50% transparency to show the tracking of individual roots in 3D space. (c) 3D visualization of the root topologic structure graph consisting of all tracked trajectories. The structure graph encodes the arrangement of roots within the roots system as a data structure to compute on. The graph data structure includes the detected whorls and the connected brace and crown roots. Each individual root was color-coded by nodes and depth values.

During the sequential processing of all level set images, we calculate the diameters of the minimal bounding circle that covers all points in all level set images in a 2D projection. Table 1 lists all 16 root architecture traits that DIRT/3D computes.

Table 1: Description of DIRT/3D traits. Traits describe either a root system (RS) characteristic or measure an individual root (IR) within the root system.

Trait name	Trait type	Trait description	Unit
Whorl distance	RS	Distance between the last crown root whorl and first brace root whorl (Figure 1f). Typically, these two whorls are the first and second whorl from the top of an excavated maize root system	mm
Brace root angle	IR	Angle of the line fitted through 70% of the root length to the horizontal plane (Figure 1f)	degree
Brace/Crown/Lateral root diameter	IR	Average diameters of the fitted circles of the Brace/Crown/Lateral roots at the detected whorl locations (Figure 1f)	mm
Brace root length	IR	Average length of the B-splines fit to all recognized individual brace roots (Figure 1f)	mm
Number of brace/crown root	RS	Count of the brace/crown roots in the root system (Figure 1f)	count
Occupancy index of brace/crown root	RS	Sum of all brace/crown root diameters (mm) at the respective whorl location divided by the stem perimeter (mm)	ratio
Root system diameter	RS	Average of the maximum diameter of the roots system at consecutive depth intervals (Figure 1f)	mm
Root system eccentricity	RS	Ratio of the averages of minimum and maximum diameter of the roots system at consecutive depth intervals (Figure 4)	count
Root system density	RS	Average root area divided by the convex hull area at consecutive depth intervals	ratio
Excavated root system depth	RS	The number of level set images multiplied by the level set thickness (Figure 4)	mm
Root system projection radius	RS	The radius of the smallest enclosing circle, which is the projection of all individual roots closest to the convex hull of the root system on the horizontal plane.	mm
Stem diameter	-	Diameter of the circle fit through a slice of the stem (Figure 1f)	mm

3D root traits correlate at individual root and root system level

To test the accuracy and precision of DIRT/3D, we correlated the trait values measured automatically in the 3D point clouds and manually on the root crown. We validated manually measurable traits such as root system diameter, whorl distance, number of brace roots, and brace root angle. Computing the validated traits executes all coded lines of our software and covers all possible combinations of functions. Therefore, we consider the software to be validated in its calculations for other traits if the code is not changed. The correlation analysis of the each of the chosen validation traits showed r^2>0.85 and $p < 0.05$ for the Pearson test (Figure 7 a-e).

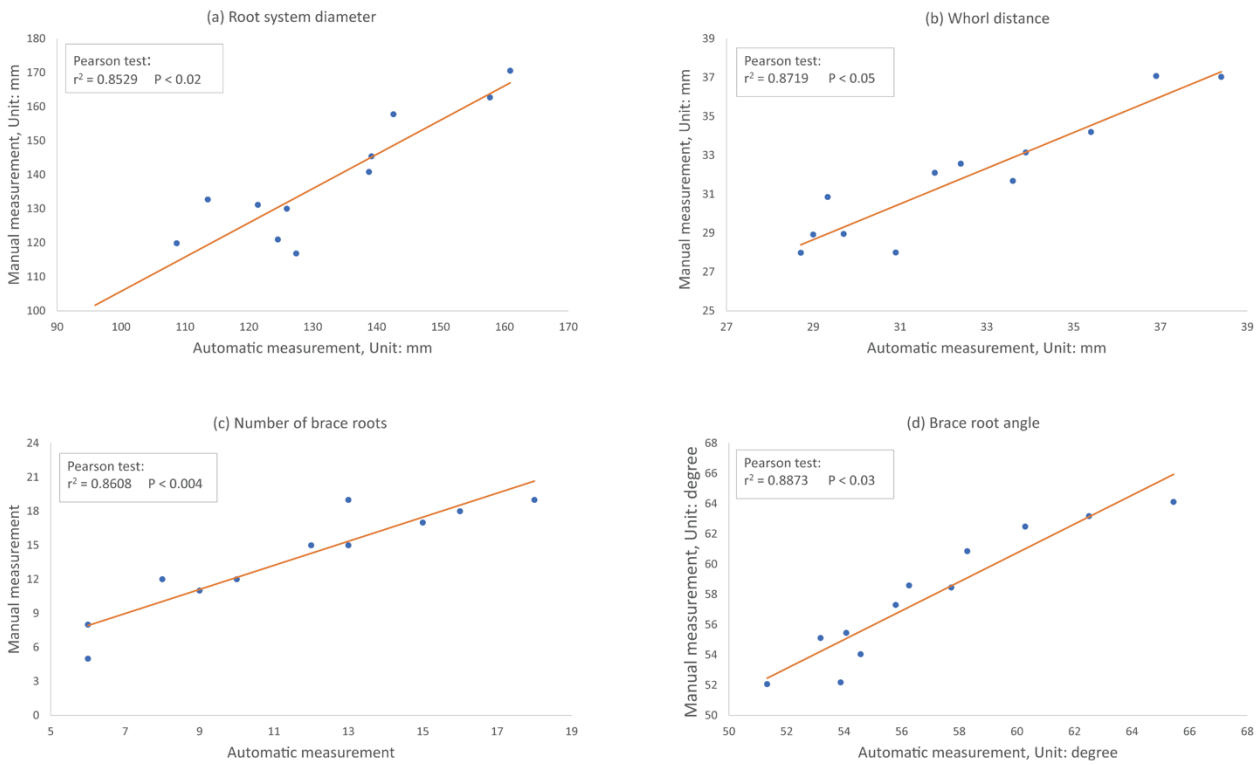

Figure 7: Correlation of automatic and manual trait measurements. Each point is the average trait value of 5-10 replicates of one of the 12 genotypes of our test panel. Pearson tests evaluated the root traits (a) the diameter of the whole root system, (b) whorl distance, defined as the distance between the brace root and crown root whorl closest to the soil line, (c) the number of brace roots, (d) brace root angle and (e) brace root diameter.

Broad sense heritability suggests high repeatability of the observed root trait values

Broad-sense heritability, H^2_{mean} for all traits (Figure 8) is computed as the ratio of total genetic variance to total phenotypic variance (Falconer 1989) to demonstrate the repeatability of the initial fields trial. For quantitative plant traits, the broad-sense heritability across multiple varieties eliminates the time-consuming steps of hybridization and population development for determining H^2_{mean}. We observed a broad-sense heritability $H^2_{mean} > 0.6$ for all traits except brace root angle, which indicates a moderately strong genetic basis of the computed traits. Seven of the computed traits resulted in $H^2_{mean} > 0.9$ (Figure 8), which indicates that the calculated traits show minimal variation within genotypes.

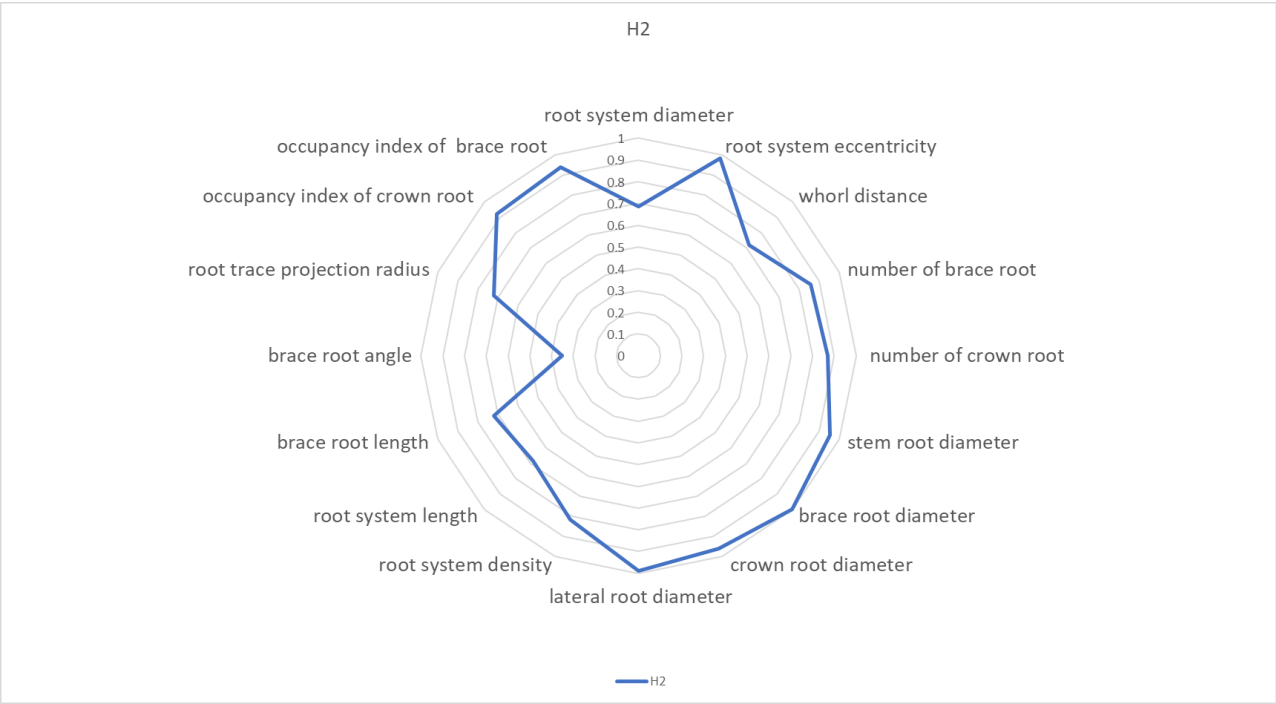

Figure 8: Broad sense heritability for all 16 computed traits. Phenotypes vary between the individuals because of both environmental factors, the genes that control traits, as well as various interactions between genes and environmental factors. We computed broad-sense heritability for all 3D traits in Table 1. All but one trait suggests a strong genetic basis to explain the observed inter-genotypic variation with $H^2_{mean} > 0.6$.

3D root traits distinguish genotypes in the test panel

The 16 computed 3D root traits distinguished genotypes by their means (Figure 9). Overall, we found that no single trait classifies all genotypes. However, an ANOVA test revealed that the means of each pair of genotypes distinguishes in at least four traits (Supplementary Material 17). For example, genotype PA762 and B101 show a significant difference with traits such as brace root diameter and lateral root diameter. However, B101, PA762, and PHG50XHG47 do not show separable mean values in the brace root angle.

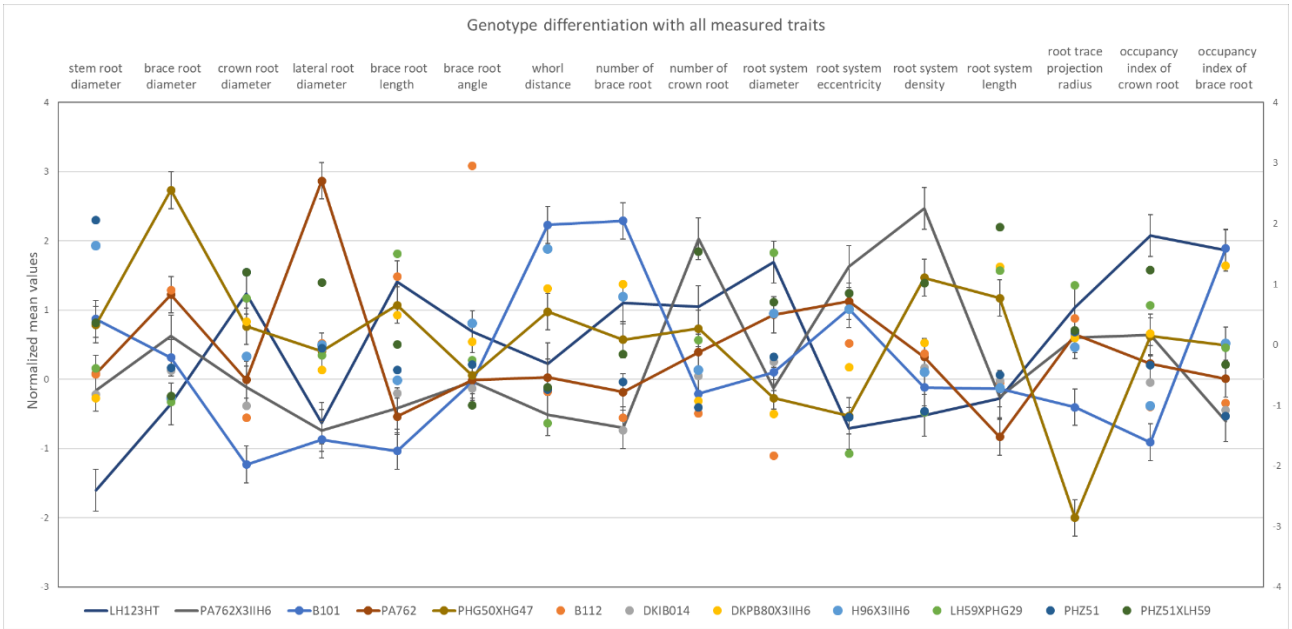

Figure 9: Genotype differentiation of 12 maize genotypes. We normalized all the mean trait values of computed 3D root traits from DRIT/3D. Colored points denote the normalized mean values of the 16 root traits. The lines guide the reader visually to explore the phenotypic variation between genotypes of the test panel. For example, the mean of genotype PA762 and B101 distinguishes in brace root diameter and lateral root diameter; Genotype PHG50XHG47 and PA762 distinguish in the root projection radius. However, B101, PA762, and PHG50XHG47 do not show distinguishing mean values in the brace root angle.

Whole root descriptor distinguishes the unique spatial arrangement of individual roots for all genotypes

We introduce a 3D variation of the established D-curve for 2D images (Bucksch, Burridge et al. 2014) as a whole root descriptor. We compute the descriptor from the sequence of level set images derived from the reconstructed 3D root models. For each level set image, we compute the number of pixels that represent roots as a measure for the area. We found that the accumulation of root area across the level-set images is an intrinsic characteristic of each genotype (Supplementary Material 10). The descriptor is robust to outliers and measurement errors because it relies on the cumulative distribution function (Chun, Han et al. 2000, Lee 2001, Kyurkchiev 2015). Figure 9 shows the results of the test panel of the 12 genotypes used the maize test panel. The whole root descriptor distinguished the unique arrangement of individual roots for all 12 genotypes as a characteristic mean curve, as shown in Figure 10.

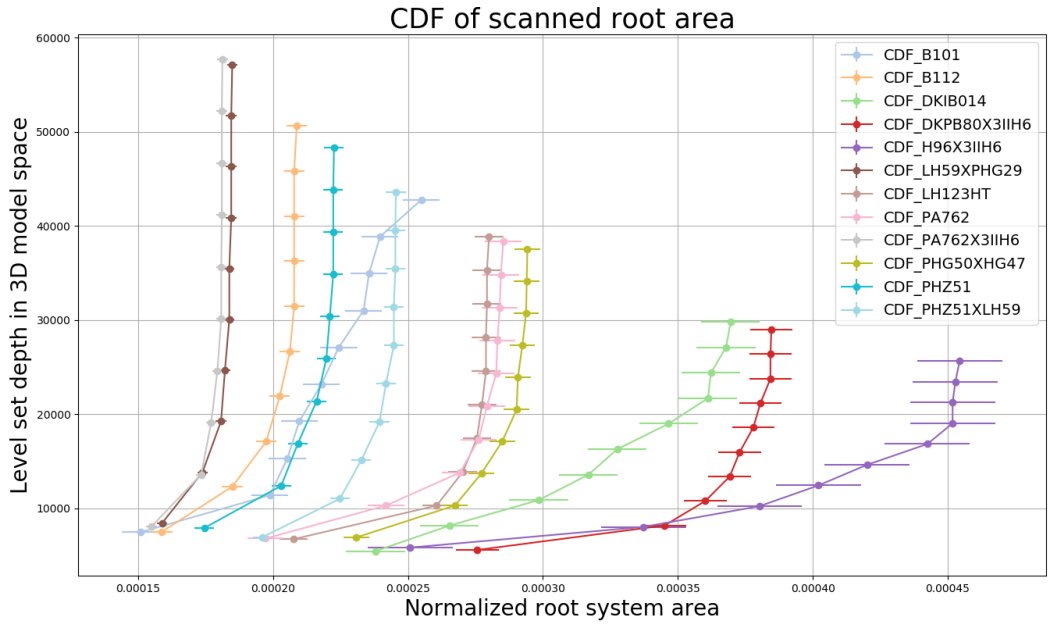

Figure 10: The whole root descriptor of all 12 maize genotypes of the test panel. The descriptor encodes the spatial arrangement of individual roots within the root system as a function of the excavation depth. We define the curve of the cumulative root system area as the cumulative distribution function (CDF) of the area per level set for each genotype. The error bar denotes the standard error of the normalized root area. Each genotype associates with a characteristic CDF curve (colored coded). All genotypes distinguish visually from each other in their curve characteristics.

Discussion

The presented 3D system to measure traits in highly occluded root systems is a significant advance in root phenotyping because it measures highly occluded traits such as whorl distance and number or brace and crown roots in the dense maize root system. Furthermore, the presented methods push against the frontier of phenomics by presenting a whole root descriptor for plant root architecture. For the test panel of twelve genotypes, a minimum of four traits distinguished all genotypes. In contrast, the whole root descriptor is one characteristic that distinguished all genotypes with one mathematical expression. Both together, put forward the unaccomplished goal of phenomics to measure the comprehensive appearance of a continuously reshaping phenotype (Houle, Govindaraju et al. 2010).

However, some algorithmic and technical challenges remain to exploit the utility of 3D root phenotyping for breeders fully. To date, standard calibration procedures for structure from motion scanners with multiple cameras are rare (Conte, Girelli et al. 2018). Further research will focus on the details of the photogrammetric calibration of the 3D root scanner, which will allow for thinner cross-section slices during level set extraction. We believe that root models of higher resolution will enable the reconstruction of a more detailed root architecture to obtain measures of all nodes in the maize root system.

We demonstrated the possibility to retrieve high geometric detail from field excavated roots. We even argue that it will be possible to obtain geometrically complete measurements in the sense of Euclid's definitions in Elements I-IV and VI (Casey 2015). Local measurements of length, diameter, and angle are sufficient to reconstruct every solid 3D object if sampled at sufficiently high rates. Again, research on the calibration technique used for structure from motion scanners seems likely to be the limiting factor in achieving the needed resolution. Assembling the complete geometrical system of the root system will allow us to describe the whole root system and its spatial arrangements

in one single mathematical construct. We presented a first 3D whole root descriptor that is similar to the validated D- and DS-curve for 2D images (Bucksch, Burridge et al. 2014). We encoded root architecture as an aggregate of the extracted 3D traits and could reliably distinguish the roots of different genotypes for a small diversity panel. However, our approach neglects root density and root order, which limits the encoded detail. An extension of the presented whole root descriptor would enable the quantification of morphological differences within homozygous populations to understand the variation of architecture arrangements. Besides, the comparison between plant species with similar topological organization but different geometric growth such as dense first order laterals yet with varying patterns of curvature along the root, would be enabled.

The observed broad-sense heritability suggests a strong repeatability of our first study ($H^2_{mean} > 0.7$ for most traits). Repeatability, paired with near geometric completeness, indicates the presence of a local and global architecture control by genes. Local control relates to phenes that assemble the architectural phenome of roots as a set of mappable and locally measurable traits (Lynch and Brown 2012). However, it is still an open question if a "global control phene" of root architecture phenes exists (Jiang, Floro et al. 2019) unless we can map whole root architectures that are geometrically complete. A necessary step towards answering this question from a mathematical point of view is to define a mathematical basis of locally controlled traits or phenes. Since phenes are often mappable to genes (Yablokov 1986), a mathematically independent basis formed by phenes would open ways for the alternative hypothesis that roots have access to a spectrum of architectures that acclimatize to their micro- and macro-environments via their species-specific phenes.

Conclusion

Our 3D phenotyping system is arguably the first optical system to handle highly occluded and mature root systems in the field. It is worth noting that the time required to collect the imaging data is around five minutes, which is significantly less than a typical X-Ray scan at a comparable resolution (Paya, Silverberg et al. 2015). Unlike many root phenotyping methods developed under lab conditions, our system measures maize roots grown under field conditions. We also demonstrated that our system reliably computes previously inaccessible traits, such as whorl distance, and the number and angles of both brace and crown roots. We validated our system for the root trait classes of number, angle, diameter, and length. Validation results demonstrate the reliability of our system with correlations of $r^2 > 0.84$ for most traits and P-values < 0.005. From our analysis, we concluded that DIRT/3D could extract 3D root traits accurately at the individual and system levels.

Our open-source software is available to the whole plant science community on GitHub, and can be deployed within a platform-agnostic Singularity container to be executed independently of the operating system (Supplementary Material 11) (https://github.com/Computational-Plant-Science). The use of Singularity containers will allow for integration with cyber-infrastructures such as CyVerse. These containers can run on any high-performance computing system that has the Singularity environment installed.

The only user interaction in our system is to place the root in the scanner, which could be replaced by a robot. Hence, we see our system as the first milestone towards automated root trait measurements in the field. Our belief stems from ongoing developments in agricultural robotics that will excavate field roots "on-the-go" (Shi, Choi et al. 2019) in the foreseeable future. In that way, our system supports breeders and root biologists in the development of crops with increased water uptake, more efficient nitrogen capture and improved sequestration of atmospheric carbon to mitigate the adverse effects of climate change without compromising on yield gains.

Material and Methods

Plant material

Plants were grown at The Pennsylvania State University's Russell E. Larson Agricultural Research Center (40° 42'40.915" N, 77°, 57'11.120''W) which has a Hagerstown silt loam soil (fine, mixed, semi-active, mesic Typic Hapludalf). Fields received fertilization with 190 kg nitrogen ha^{-1} applied as urea (46-0-0). The sites had drip irrigation.

The field management supplemented nutrients other than nitrogen, and applied pest management as needed. We planted seeds using hand jab planters in rows with 76 cm row spacing, 91 cm alleys, 23 cm plant spacing, 4.6 m plot length with 3.7 m planted, or ~56,800 plants ha^{-1}. We grew plants in three-row plots, and sampled only the middle row. Planting occurred on June 5, 2018, and sampling on August 25, 2018, 81 days after planting. Two fields provided 1ha of space for four replicates.

Twelve genotypes were selected based on previous knowledge of their architectural variation and sampling of a larger set of genotypes. The twelve genotypes included six inbred lines (B101, B112, DKIB014, LH123HT, Pa762, PHZ51) and six hybrid lines (DKPB80 x 3IIH6, H96 x 3IIH6, LH59 x PHG29, Pa762 x 3IIH6, PHG50 x PHG47, PHZ51 x LH59). These genotypes represent the extremes of dense vs. sparse, large vs. small, and maximum and minimum number of whorls selected from a full diversity panel. The lab of Shawn Kaeppler at the University of Wisconsin provided the seeds. We selected ten representative plants for five of the genotypes (B112, Pa762, PHZ51, DKPB80 x 3IIH6, H96 x 3IIH6), and five plants of the remaining seven genotypes. Sampling followed the shovelomics protocol (Trachsel et al., 2011. We air-dried the roots on a greenhouse bench and then transported the roots to the lab for imaging.

3D root scanner

We designed a 3D root scanner (Figure 2a) to capture images for 3D reconstruction of the root (Supplementary Material 3). A stepper motor (Nema 34 CNC High Torque Stepper Motor 13Nm with Digital Stepper Driver DM860I, Figure 2b) rotates a curved metal frame with ten low cost and highly versatile imaging cameras (Image Source DFK 27BUJ003 USB 3.0) around the clamped root crown in a central fixture (Figure 2c). From the stepper motor, we chose 12800 micro-step resolutions to rotate in 1-degree steps (Figure 2b). The cameras ship with the 1/2.3" Aptina CMOS MT9J003 sensor and can achieve high image resolution at 3,856×2,764 (10.7 MP) up to 7 fps. We drilled 21 equidistant holes into the curved frame to provide a flexible arrangement of each camera. A rail track along the curved frame allows for fine adjustment of the camera tilt and pan direction without compromising stability (Figure 2d).

A computing cluster of ten Raspberry Pi 3 B+ synchronizes the image capture of the ten cameras using a master-slave design (Supplementary Material 12). The synchronized cameras of our 3D root scanner capture approximately 2000 images per maize root in about 5 min. The newly developed controller software on the raspberry pi computing cluster synchronizes the camera's image capture and the step motor movement. Once the step motor receives the "start move" signal via the master unit, it moves all the cameras into their designated positions. Then, all ten cameras capture images simultaneously. Each Raspberry Pi stores the image initially on a sim card. During the image capturing process, the step motor stands still and waits for the next "start move" signal. The image data of all Raspberry Pi's automatically transfers to the Cyverse Data Store (Center 2011, Merchant, Lyons et al. 2016). Only the master unit stores information about the Cyverse user account. It uses the iRods protocol (Ward, de Torcy et al. 2009) to transfer the images from each slave unit to the Cyverse Data Store. In the following, the 3D reconstruction uses the image data in the online storage to generate the 3D point cloud of the root system. Alternatively, the image data can be transferred manually to computers within the same WiFi network.

Automatic reconstruction of the 3D root model with structure-from-motion

Illumination adjustment and content-based segmentation to remove redundant information

We use standard deviation and a luminance-weighted gray world algorithm (Lam 2005) to adjust and normalize illumination across all captured images. The root is automatically separated from the background using a newly developed content-based segmentation method (Supplementary Material 13). The method analyzes and compares color-space differences across all normalized images and omits the redundant information of the background. Overall, the size of the image data reduces to 30-50% of the original size. In later steps of the pipeline, the segmentation decreases the number of false feature matchings computed in the 3D reconstruction process as well

as the amount of data transmitted to online storage. The method is fully automatic and parameter-free and uses parallel processing if available.

Improved feature matching to reduce computation time and improve 3D point cloud resolution

Given the images of segmented roots, we chose the Visual Structure From Motion method (Wu 2011) as a basis to develop 3D reconstruction software for roots. The computationally most expensive aspect of structure-from-motion algorithms is the feature matching between image pairs. The amount and accuracy of the feature matching determines the quality and resolution of the resulting 3D root model. In the original version, Visual Structure from Motion performs a full pairwise image matching to build a feature space across all possible image pairs. For example, the number of permutations P calculates for r images out of a set of n total images with the following formula:

$$P_n^r = \frac{n!}{(n-r)!}$$

However, the computation of feature matches generates a large amount of false feature correspondences in the dense root data. We found that image pairs that are not adjacent in the spherical scanner space are particularly prone to incorrect matching (Supplementary Material 14). We observed that the false feature matches occur predominantly between the dense and thin roots of the root system. Therefore, we optimized the feature matching process to be suitable for dense root architectures.

The optimization in our algorithm generates a matching pair list inside a specified sliding window (Supplementary Material 15). Sliding of the window allows for robust matching among all permutations of image pairs. For example, given an image set captured around the individual root in the 1-degree interval (360 images in total), we set the sliding window size as 10% of the image size. The widow size was found experimentally and is the optimum for the 1-degree interval setting of the scanner. The total number of permutations of image pairs needed for feature matching is $\frac{360!}{(360-2)!} = 129{,}240$ according to the formula above. For an image of size 1000 ×1000, we set the sliding window size as 100×100, the number of permutations of image pairs needed will be reduced to $\frac{100!}{(100-2)!} = 2450$. In that way, we need to compute only 1.89% of all permutations of image pairs.

As a next step, we utilize the RANSAC (random sample consensus) method to detect and remove the falsely matched pairs. The RANSAC results usually contain only highly distinctive features to track between consecutive images. Given the locations of multiple matched feature pairs in two or more images, we can produce an estimation of the positions, orientations of cameras, and the coordinates of the features in a single step using bundle adjustment (Wu, Agarwal et al. 2011).

Computing root traits from 3D models

We adopted a top-down level set scan of the 3D root model to compute 3D root traits (Supplementary Material 16). This scanning process generates a thin vertical 2D slice or level set image given a fixed plane. We use a phase-based frame interpolation technique from video processing to smooth the image sequence. We developed a method to extract individual roots in each level set image using the active contour snake model. Then we use the watershed segmentation to segment the overlapping roots. Given a smoothed and segmented level set image sequence, we used a combination of Kalman filters and the Hungarian algorithm (Sahbani and Adiprawita 2016) to track all the individual roots, and build a graph of the root topologic structure and computed all 16 root system architecture traits.

Statistical Analyses

All statistics used python 3.7 and the modules NumPy 1.16 and SciPy 1.2.1 (Oliphant 2007). Figures 7 and 10 used matplotlib 3.2.1 (Hunter 2007) for visualization of the statistics. Figures 8 and 9 used Microsoft Excel Version 16.34 to visualize trait and heritability data. Raw data are available in (Supplementary Material 17).

ACKNOWLEDGMENTS

The research was supported by the USDOE ARPA-E ROOTS Award Number DE-AR0000821 to A.B. and J.P.L.. The work was supported in part by the NSF CAREER Award No. *1845760* to A.B. Any Opinions, findings, and conclusions or recommendations expressed in this material are those of the author(s) and do not necessarily reflect those of the National Science Foundation. This work used the Extreme Science and Engineering Discovery Environment (XSEDE) resource Stampede2 at the Texas Advanced Computing Center through allocation TG-BIO160088. This material is partly based upon work supported by the National Science Foundation under Award Numbers DBI-0735191, DBI-1265383, and DBI-1743442. URL: www.cyverse.org.

CONTRIBUTIONS

S.L. wrote the manuscript, designed and implemented algorithms, designed and built hardware, performed data analysis and contributed to the experimental design. C.B.S. designed and built hardware. J.P.L. contributed to writing of the manuscript and the project idea, conceived experimental design. M.H. contributed to writing the manuscript, performed experiments and collected data. A.B. conceived the project idea, designed hardware, contributed to the data analysis, wrote manuscript and designed algorithms.

REFERENCES

Arifuzzaman, M., A. Oladzadabbasabadi, P. McClean and M. Rahman (2019). "Shovelomics for phenotyping root architectural traits of rapeseed/canola (Brassica napus L.) and genome-wide association mapping." Molecular Genetics and Genomics: 1-16.

Ault, T. R. (2020). "On the essentials of drought in a changing climate." Science **368**(6488): 256-260.

Bourgault, M., A. T. James and M. F. Dreccer (2017). "Pot size matters revisited: Does container size affect the response to elevated CO2 and our ability to detect genotypic variability in this response in wheat?" Functional Plant Biology **44**(1): 52-61.

Bray, A. L. and C. N. Topp (2018). "The quantitative genetic control of root architecture in maize." Plant and Cell Physiology **59**(10): 1919-1930.

Bucksch, A. (2011). Revealing the skeleton from imperfect point clouds. Munchen, Dr. Hut.

Bucksch, A. (2014). "A practical introduction to skeletons for the plant sciences." Applications in plant sciences **2**(8): 1400005.

Bucksch, A., A. Atta-Boateng, A. F. Azihou, D. Battogtokh, A. Baumgartner, B. M. Binder, S. A. Braybrook, C. Chang, V. Coneva, T. J. DeWitt, A. G. Fletcher, M. A. Gehan, D. H. Diaz-Martinez, L. Hong, A. S. Iyer-Pascuzzi, L. L. Klein, S. Leiboff, M. Li, J. P. Lynch, A. Maizel, J. N. Maloof, R. J. C. Markelz, C. C. Martinez, L. A. Miller, W. Mio, W. Palubicki, H. Poorter, C. Pradal, C. A. Price, E. Puttonen, J. B. Reese, R. Rellan-Alvarez, E. P. Spalding, E. E. Sparks, C. N. Topp, J. H. Williams and D. H. Chitwood (2017). "Morphological Plant Modeling: Unleashing Geometric and Topological Potential within the Plant Sciences." Front Plant Sci **8**: 900.

Bucksch, A., J. Burridge, L. M. York, A. Das, E. Nord, J. S. Weitz and J. P. Lynch (2014). "Image-based high-throughput field phenotyping of crop roots." Plant Physiology **166**(2): 470-486.

Bucksch, A., A. Das, H. Schneider, N. Merchant and J. S. Weitz (2017). "Overcoming the Law of the Hidden in Cyberinfrastructures." Trends Plant Sci **22**(2): 117-123.

Burridge, J., C. N. Jochua, A. Bucksch and J. P. Lynch (2016). "Legume shovelomics: high—throughput phenotyping of common bean (Phaseolus vulgaris L.) and cowpea (Vigna unguiculata subsp, unguiculata) root architecture in the field." Field Crops Research **192**: 21-32.

Busener, N., J. Kengkanna, P. J. Saengwilai and A. Bucksch (2020). "Image-based root phenotyping for plant breeding to improve the nutritional quality of cassava." Plants, People, Planet **(under revision)**.

Casey, J. (2015). Euclid's" Elements" Redux, John Casey.

Center, D. (2011). "The iPlant collaborative: cyberinfrastructure for plant biology." Chardon, M., and Vandewalle, P.(1991). Acoustico-lateralis system. Cyprinid Fishes.

Chun, M.-H., S.-J. Han and N.-I. Tak (2000). "An uncertainty importance measure using a distance metric for the change in a cumulative distribution function." Reliability Engineering & System Safety **70**(3): 313-321.

Clark, R. T., R. B. MacCurdy, J. K. Jung, J. E. Shaff, S. R. McCouch, D. J. Aneshansley and L. V. Kochian (2011). "Three-dimensional root phenotyping with a novel imaging and software platform." Plant physiology **156**(2): 455-465.

Cochard, H., S. Delzon and E. Badel (2015). "X-ray microtomography (micro-CT): a reference technology for high-resolution quantification of xylem embolism in trees." Plant, Cell & Environment **38**(1): 201-206.

Colombi, T., N. Kirchgessner, C. A. Le Marié, L. M. York, J. P. Lynch and A. Hund (2015). "Next generation shovelomics: set up a tent and REST." Plant and Soil **388**(1-2): 1-20.

Conte, P., V. A. Girelli and E. Mandanici (2018). "Structure from Motion for aerial thermal imagery at city scale: Pre-processing, camera calibration, accuracy assessment." ISPRS journal of photogrammetry and remote sensing **146**: 320-333.

Das, A., H. Schneider, J. Burridge, A. K. M. Ascanio, T. Wojciechowski, C. N. Topp, J. P. Lynch, J. S. Weitz and A. Bucksch (2015). "Digital imaging of root traits (DIRT): a high-throughput computing and collaboration platform for field-based root phenomics." Plant methods **11**(1): 51.
Dinas, P. C., A. Nikaki, A. Z. Jamurtas, V. Prassopoulos, R. Efthymiadou, Y. Koutedakis, P. Georgoulias and A. D. Flouris (2015). "Association between habitual physical activity and brown adipose tissue activity in individuals undergoing PET-CT scan." Clinical endocrinology **82**(1): 147-154.
Fabbri, R., L. D. F. Costa, J. C. Torelli and O. M. Bruno (2008). "2D Euclidean distance transform algorithms: A comparative survey." ACM Computing Surveys (CSUR) **40**(1): 2.
Falconer, D. S. (1989). Introduction to Quantiative Genetics 3rd Edition. Essex, UK, Longman Scientific & Technical.
Falk, K. G., T. Z. Jubery, S. V. Mirnezami, K. A. Parmley, S. Sarkar, A. Singh, B. Ganapathysubramanian and A. K. Singh (2020). "Computer vision and machine learning enabled soybean root phenotyping pipeline." Plant Methods **16**(1): 5.
Fischer, A., T. Lasser, M. Schrapp, J. Stephan and P. B. Noël (2016). "Object specific trajectory optimization for industrial X-ray computed tomography." Scientific reports **6**: 19135.
Galkovskyi, T., Y. Mileyko, A. Bucksch, B. Moore, O. Symonova, C. A. Price, C. N. Topp, A. S. Iyer-Pascuzzi, P. R. Zurek and S. Fang (2012). "GiA Roots: software for the high throughput analysis of plant root system architecture." BMC plant biology **12**(1): 116.
Gray, S. B., R. S. Strellner, K. K. Puthuval, C. Ng, R. E. Shulman, M. H. Siebers, A. Rogers and A. D. Leakey (2013). "Minirhizotron imaging reveals that nodulation of field-grown soybean is enhanced by free-air CO2 enrichment only when combined with drought stress." Functional Plant Biology **40**(2): 137-147.
Grift, T. E., J. Novais and M. Bohn (2011). "High-throughput phenotyping technology for maize roots." Biosystems engineering **110**(1): 40-48.
Houle, D., D. R. Govindaraju and S. Omholt (2010). "Phenomics: the next challenge." Nat Rev Genet **11**(12): 855-866.
Hunter, J. D. (2007). "Matplotlib: A 2D Graphics Environment." Computing in Science & Engineering **9**: 90-95.
Hyun, S.-J., C.-W. Bae, S.-H. Lee and S.-C. Rhim (2016). "Fatty degeneration of the paraspinal muscle in patients with degenerative lumbar kyphosis: a new evaluation method of quantitative digital analysis using MRI and CT scan." Clinical spine surgery **29**(10): 441-447.
Iyer-Pascuzzi, A. S., O. Symonova, Y. Mileyko, Y. Hao, H. Belcher, J. Harer, J. S. Weitz and P. N. Benfey (2010). "Imaging and analysis platform for automatic phenotyping and trait ranking of plant root systems." Plant physiology **152**(3): 1148-1157.
Jahnke, S., M. I. Menzel, D. Van Dusschoten, G. W. Roeb, J. Bühler, S. Minwuyelet, P. Blümler, V. M. Temperton, T. Hombach and M. Streun (2009). "Combined MRI–PET dissects dynamic changes in plant structures and functions." The Plant Journal **59**(4): 634-644.
Jiang, N., E. Floro, A. L. Bray, B. Laws, K. E. Duncan and C. N. Topp (2019). "Three-dimensional time-lapse analysis reveals multiscale relationships in maize root systems with contrasting architectures." The Plant Cell **31**(8): 1708-1722.
Kass, M., A. Witkin and D. Terzopoulos (1988). "Snakes: Active contour models." International journal of computer vision **1**(4): 321-331.
Kengkanna, J., P. Jakaew, S. Amawan, N. Busener, A. Bucksch and P. Saengwilai (2019). "Phenotypic variation of cassava root traits and their responses to drought." Applications in plant sciences **7**(4): e01238.

Keyes, S. D., K. R. Daly, N. J. Gostling, D. L. Jones, P. Talboys, B. R. Pinzer, R. Boardman, I. Sinclair, A. Marchant and T. Roose (2013). "High resolution synchrotron imaging of wheat root hairs growing in soil and image based modelling of phosphate uptake." New Phytologist **198**(4): 1023-1029.
Kuijken, R. C., F. A. van Eeuwijk, L. F. Marcelis and H. J. Bouwmeester (2015). "Root phenotyping: from component trait in the lab to breeding." Journal of experimental botany **66**(18): 5389-5401.
Kurtzer, G. M., V. Sochat and M. W. Bauer (2017). "Singularity: Scientific containers for mobility of compute." PloS one **12**(5): e0177459.
Kyurkchiev, N. (2015). "On the Approximation of the step function by some cumulative distribution functions." Compt. rend. Acad. bulg. Sci **68**(12): 1475-1482.
Lam, E. Y. (2005). Combining gray world and retinex theory for automatic white balance in digital photography. Proceedings of the Ninth International Symposium on Consumer Electronics, 2005.(ISCE 2005). IEEE.
Lee, H.-s. (2001). Method and circuit for extracting histogram and cumulative distribution function for image enhancement apparatus, Google Patents.
Lobet, G., L. Pagès and X. Draye (2011). "A novel image-analysis toolbox enabling quantitative analysis of root system architecture." Plant physiology **157**(1): 29-39.
Lynch, J. P. (2013). "Steep, cheap and deep: an ideotype to optimize water and N acquisition by maize root systems." Ann Bot **112**(2): 347-357.
Lynch, J. P. (2019). "Root phenotypes for improved nutrient capture: an underexploited opportunity for global agriculture." New Phytologist **223**(2): 548-564.
Lynch, J. P. and K. M. Brown (2012). "New roots for agriculture: exploiting the root phenome." Philos Trans R Soc Lond B Biol Sci **367**(1595): 1598-1604.
Lynch, J. P. and K. M. Brown (2012). "New roots for agriculture: exploiting the root phenome." Philosophical Transactions of the Royal Society B: Biological Sciences **367**(1595): 1598-1604.
Lynch, J. P. and T. Wojciechowski (2015). "Opportunities and challenges in the subsoil: pathways to deeper rooted crops." Journal of Experimental Botany **66**(8): 2199-2210.
Merchant, N., E. Lyons, S. Goff, M. Vaughn, D. Ware, D. Micklos and P. Antin (2016). "The iPlant collaborative: cyberinfrastructure for enabling data to discovery for the life sciences." PLoS biology **14**(1): e1002342.
Metzner, R., A. Eggert, D. van Dusschoten, D. Pflugfelder, S. Gerth, U. Schurr, N. Uhlmann and S. Jahnke (2015). "Direct comparison of MRI and X-ray CT technologies for 3D imaging of root systems in soil: potential and challenges for root trait quantification." Plant methods **11**(1): 17.
Meyer, S., O. Wang, H. Zimmer, M. Grosse and A. Sorkine-Hornung (2015). Phase-based frame interpolation for video. Proceedings of the IEEE conference on computer vision and pattern recognition.
Moghaddam, R. F. and M. Cheriet (2012). "AdOtsu: An adaptive and parameterless generalization of Otsu's method for document image binarization." Pattern Recognition **45**(6): 2419-2431.
Mugerwa, H., M. E. C. Rey, F. Tairo, J. Ndunguru and P. Sseruwagi (2019). "Two sub-Saharan Africa 1 populations of Bemisia tabaci exhibit distinct biological differences in fecundity and survivorship on cassava." Crop Protection **117**: 7-14.
Nagel, K. A., A. Putz, F. Gilmer, K. Heinz, A. Fischbach, J. Pfeifer, M. Faget, S. Blossfeld, M. Ernst and C. Dimaki (2012). "GROWSCREEN-Rhizo is a novel phenotyping robot enabling simultaneous measurements of root and shoot growth for plants grown in soil-filled rhizotrons." Functional Plant Biology **39**(11): 891-904.
Oliphant, T. E. (2007). "Python for Scientific Computing." Computing in Science & Engineering **9**: 10-20.
Oliva, M. and C. Dunand (2007). "Waving and skewing: how gravity and the surface of growth media affect root development in Arabidopsis." New Phytologist **176**(1): 37-43.

Paez-Garcia, A., C. M. Motes, W.-R. Scheible, R. Chen, E. B. Blancaflor and M. J. Monteros (2015). "Root traits and phenotyping strategies for plant improvement." Plants **4**(2): 334-355.
Paustian, K., G. Agren and E. Bosatta (1997). "Modelling litter quality effects on decomposition and soil organic matter dynamics." Driven by nature: plant litter quality and decomposition.
Paustian, K., J. Lehmann, S. Ogle, D. Reay, G. P. Robertson and P. Smith (2016). "Climate-smart soils." Nature **532**(7597): 49-57.
Paya, A. M., J. L. Silverberg, J. Padgett and T. L. Bauerle (2015). "X-ray computed tomography uncovers root–root interactions: quantifying spatial relationships between interacting root systems in three dimensions." Frontiers in plant science **6**: 274.
Pfeifer, J., N. Kirchgessner, T. Colombi and A. Walter (2015). "Rapid phenotyping of crop root systems in undisturbed field soils using X-ray computed tomography." Plant methods **11**(1): 41.
Playne, D. P. and K. Hawick (2018). "A new algorithm for parallel connected-component labelling on GPUs." IEEE Transactions on Parallel and Distributed Systems **29**(6): 1217-1230.
Poorter, H., J. Bühler, D. van Dusschoten, J. Climent and J. A. Postma (2012). "Pot size matters: a meta-analysis of the effects of rooting volume on plant growth." Functional Plant Biology **39**(11): 839-850.
Poorter, H., F. Fiorani, R. Pieruschka, T. Wojciechowski, W. H. van der Putten, M. Kleyer, U. Schurr and J. Postma (2016). "Pampered inside, pestered outside? Differences and similarities between plants growing in controlled conditions and in the field." New Phytol **212**(4): 838-855.
Ranum, P., J. P. Peña-Rosas and M. N. Garcia-Casal (2014). "Global maize production, utilization, and consumption." Annals of the New York Academy of Sciences **1312**(1): 105-112.
Rellán-Álvarez, R., G. Lobet, H. Lindner, P.-L. Pradier, J. Sebastian, M.-C. Yee, Y. Geng, C. Trontin, T. LaRue and A. Schrager-Lavelle (2015). "GLO-Roots: an imaging platform enabling multidimensional characterization of soil-grown root systems." Elife **4**: e07597.
Roshanian, J., S. Yazdani and M. Ebrahimi (2016). "Star identification based on euclidean distance transform, voronoi tessellation, and k-nearest neighbor classification." IEEE Transactions on Aerospace and Electronic Systems **52**(6): 2940-2949.
Sahbani, B. and W. Adiprawita (2016). Kalman filter and iterative-hungarian algorithm implementation for low complexity point tracking as part of fast multiple object tracking system. 2016 6th International Conference on System Engineering and Technology (ICSET), IEEE.
Salungyu, J., J. Kengkanna, S. Thaitad, A. Bucksch and P. Saengwilai (2020). "Translating maize root traits from the lab to the field." Field Crops Research **(Under revision)**.
Seethepalli, A., H. Guo, X. Liu, M. Griffiths, H. Almtarfi, Z. Li, S. Liu, A. Zare, F. Fritschi and E. Blancaflor (2019). "RhizoVision Crown: An Integrated Hardware and Software Platform for Root Crown Phenotyping." bioRxiv: 569707.
Shi, X., D. Choi, P. H. Heinemann, M. Hanlon and J. Lynch (2019). RootRobot: A Field-based Platform for Maize Root System Architecture Phenotyping. 2019 ASABE Annual International Meeting, American Society of Agricultural and Biological Engineers.
Slack, S., L. M. York, Y. Roghazai, J. Lynch, M. Bennett and J. Foulkes (2018). "Wheat shovelomics II: Revealing relationships between root crown traits and crop growth." BioRxiv: 280917.
Smith, P., D. Martino, Z. Cai, D. Gwary, H. Janzen, P. Kumar, B. McCarl, S. Ogle, F. O'Mara and C. Rice (2007). "Greenhouse gas mitigation in agriculture." Philosophical transactions of the royal Society B: Biological Sciences **363**(1492): 789-813.
Sozzani, R., W. Busch, E. P. Spalding and P. N. Benfey (2014). "Advanced imaging techniques for the study of plant growth and development." Trends in plant science **19**(5): 304-310.
Symonova, O., C. N. Topp and H. Edelsbrunner (2015). "DynamicRoots: a software platform for the reconstruction and analysis of growing plant roots." PLoS One **10**(6): e0127657.

Topp, C. N., A. L. Bray, N. A. Ellis and Z. Liu (2016). "How can we harness quantitative genetic variation in crop root systems for agricultural improvement?" Journal of integrative plant biology **58**(3): 213-225.
Topp, C. N., A. S. Iyer-Pascuzzi, J. T. Anderson, C.-R. Lee, P. R. Zurek, O. Symonova, Y. Zheng, A. Bucksch, Y. Mileyko and T. Galkovskyi (2013). "3D phenotyping and quantitative trait locus mapping identify core regions of the rice genome controlling root architecture." Proceedings of the National Academy of Sciences **110**(18): E1695-E1704.
Trachsel, S., S. M. Kaeppler, K. M. Brown and J. P. Lynch (2011). "Shovelomics: high throughput phenotyping of maize (Zea mays L.) root architecture in the field." Plant and Soil **341**(1-2): 75-87.
van Dusschoten, D., R. Metzner, J. Kochs, J. A. Postma, D. Pflugfelder, J. Bühler, U. Schurr and S. Jahnke (2016). "Quantitative 3D analysis of plant roots growing in soil using magnetic resonance imaging." Plant physiology **170**(3): 1176-1188.
Waki, K. (2016). 3-dimensional elastic image generation method and ultrasonic diagnostic apparatus, Google Patents.
Ward, J. H., A. de Torcy, M. Chua and J. Crabtree (2009). Extracting and Ingesting DDI Metadata and Digital Objects from a Data Archive into the iRODS extension of the NARA TPAP using the OAI-PMH. 2009 Fifth IEEE International Conference on e-Science, IEEE.
Wu, C. (2011). "VisualSFM: A visual structure from motion system."
Wu, C., S. Agarwal, B. Curless and S. M. Seitz (2011). Multicore bundle adjustment. CVPR 2011, IEEE.
Yablokov, A. V. (1986). Phenetics - Evolution, Population, Trait, Columbia University Press.
York, L. M., S. Slack, M. J. Bennett and M. J. Foulkes (2018). "Wheat shovelomics I: A field phenotyping approach for characterising the structure and function of root systems in tillering species." BioRxiv: 280875.
Yu, G., A. Zare, H. Sheng, R. Matamala, J. Reyes-Cabrera, F. B. Frischi and T. E. Juenger (2019). "Root Identification in Minirhizotron Imagery with Multiple Instance Learning." arXiv preprint arXiv:1903.03207.
Zhao, F., Q. He and J. Luo (2018). Cardiac Deformation Imaging Based on Coherent Compounding of Diverging Waves with Coded Excitation. 2018 IEEE International Ultrasonics Symposium (IUS), IEEE.
Zheng, Z., S. Hey, T. Jubery, H. Liu, Y. Yang, L. Coffey, C. Miao, B. Sigmon, J. Schnable and F. Hochholdinger (2020). "Shared genetic control of root system architecture between Zea mays and Sorghum bicolor." Plant physiology.
Zhu, J., P. A. Ingram, P. N. Benfey and T. Elich (2011). "From lab to field, new approaches to phenotyping root system architecture." Current opinion in plant biology **14**(3): 310-317.